AGU PUBLICATIONS

Geophysical Research Letters

RESEARCH LETTER
10.1002/2017GL076009

Key Points:
- Langmuir circulation is simulated with N-S equations under explicit, freely propagating surface waves
- Langmuir circulation simulated with C-L equations agrees well with the N-S simulation but is weaker
- A viscosity-induced Eulerian mean drift needs to be considered when C-L equations are used

Correspondence to:
P. Wang,
wangpeng@miami.edu

Citation:
Wang, P., & Özgökmen, T. M. (2018). Langmuir circulation with explicit surface waves from moving-mesh modeling. *Geophysical Research Letters*, *45*, 216–226. https://doi.org/10.1002/2017GL076009

Received 12 OCT 2017
Accepted 1 DEC 2017
Accepted article online 11 DEC 2017
Published online 4 JAN 2018

©2017. American Geophysical Union. All Rights Reserved.

Langmuir Circulation With Explicit Surface Waves From Moving-Mesh Modeling

P. Wang[1,2] **and T. M. Özgökmen**[1]

[1]Rosenstiel School of Marine and Atmospheric Sciences, University of Miami, Miami, FL, USA, [2]Department of Atmospheric and Oceanic Sciences, University of California, Los Angeles, CA, USA

Abstract Using a moving-mesh, nonhydrostatic, spectral element model, we simulate Langmuir circulation with Navier-Stokes equations under explicit, freely propagating surface waves. For comparison, Langmuir circulation is also simulated with Craik-Leibovich (C-L) equations. In both simulations, the Langmuir circulations are very similar, including temporal formation progresses and spatial structures; however, the strength of Langmuir circulation in the C-L simulation is a bit weaker, which we suggest is due to the lack of Eulerian mean drift induced by fluid viscosity in the presence of explicit surface waves.

1. Introduction

Langmuir circulation is named after Irving Langmuir who wrote the first scientific paper on windrows of floating weeds frequently observed in oceans and lakes (Langmuir, 1938). Conceptually, Langmuir circulation is a set of counter-rotating vortices with their rotation axis parallel to the wind direction (e.g., Leibovich, 1983; Smith, 2001; Sullivan & McWilliams, 2010; Thorpe, 2004). Langmuir circulation accumulates floating materials (e.g., oil slicks, seaweeds, and foams) into narrow bands at the surface, inhibiting the lateral dispersion (e.g., Thorpe, 2004; Yang et al., 2014) while it increases the vertical mixing of materials and momentum in upper mixed layers, such as temperature, salinity, dissolved gases (e.g., Kukulka et al., 2009; McWilliams & Sullivan, 2000), and turbulent kinetic energy (TKE) (e.g., D'Asaro et al., 2014; Harcourt & D'Asaro, 2008). Particularly in shallow waters, Langmuir circulation can penetrate full water columns under strong winds, forming "Langmuir supercells" that impact sediment transport (Gargett et al., 2004, 2014) and that cause a near-bottom intensification of downwind jets (Gargett & Wells, 2007).

Based on wave-current interaction, Craik and Leibovich (1976) proposed the most compelling explanation of Langmuir circulation and formulated the Craik-Leibovich (C-L) equations to predict Langmuir circulation. A key component of C-L equations is the term of vortex force, which is expressed as the cross product of the Stokes drift due to waves and the vorticity of background Eulerian currents. C-L equations do not explicitly resolve surface waves but instead adopt Stokes drifts solely to represent wave effects.

C-L equations are derived with the assumption of small wave slopes, which excludes breaking waves (e.g., Craik & Leibovich, 1976). In fact, breaking waves can interact with Langmuir circulation (e.g., Sullivan et al., 2004) and cause vigorous transfer and dissipation of energy (e.g., Melville, 1996). Thus, effects of breaking waves have to be included to accurately predict Langmuir circulation (e.g., S. Li et al., 2013; Noh et al., 2004; Sullivan et al., 2004, 2007; Uchiyama et al., 2010).

Much of our understanding of Langmuir circulation comes from large eddy simulations (LES) based on C-L equations (e.g., McWilliams et al., 1997; Skyllingstad & Denbo, 1995); hence, the verification of C-L equations becomes an important task. From the point of view of mathematical derivations, C-L equations derived using the method of asymptotic expansion (e.g., Craik & Leibovich, 1976; Lane et al., 2007; McWilliams & Restrepo, 1999; McWilliams et al., 2004) are consistent with those derived using methods of generalized Lagrangian mean (e.g., Andrews & McIntyre, 1978; Ardhuin et al., 2008) and Hamiltonian principle (Gjaja & Holm, 1996; Holm, 1996). On the contrary, Mellor (2016) holds a different opinion on the correctness of C-L equations.

In addition to mathematical comparisons, there are also numerical comparisons of Langmuir circulation simulated with C-L and N-S equations (e.g., Ferziger et al., 2002; Kawamura, 2000; Zhou, 2000), but those

comparisons are unsatisfactory, because they use either nondeforming, rigid surface waves or constant Stokes drifts with the underlying assumption of unaffected waves by currents. These drawbacks are overcome in our study. Using a moving-mesh, nonhydrostatic model, we compare Langmuir circulations between C-L and N-S equations in the context of explicit, freely propagating, dynamically deforming surface waves of small wave slopes; in particular, our waves contain effects of currents.

2. Methods

The numerical simulations are conducted with Nek5000 (Fischer, 1997), which solves incompressible, nonhydrostatic N-S equations using the spectral element method (Patera, 1984). Nek5000 decomposes numerical domains into hexahedral elements (e.g., Figure 1a). Within each element, solutions are constructed by polynomials on Gauss-Lobatto-Legendre (GLL) quadrature points. Nek5000 has been employed to study various kinds of oceanic flows, such as the material transport inside an ocean eddy (Pratt et al., 2014; Rypina et al., 2015; Wang & Özgökmen, 2015), spiral inertial waves emitted from unstable ocean eddies (Wang & Özgökmen, 2016), and material dispersion by oceanic internal waves (Wang et al., 2016).

We conduct two sets of numerical simulations, that is, one with N-S equations and the other with C-L equations. In the N-S simulation, moving meshes are employed to model oscillating motions of surface waves, while in the C-L simulation, static meshes are used since no explicit surface waves are presented.

2.1. N-S Moving-Mesh Simulation

Nek5000 integrates the incompressible N-S equations:

$$\frac{\partial \mathbf{u}}{\partial t} + (\mathbf{u}\cdot\nabla)\mathbf{u} = -\frac{1}{\rho}\nabla p + \nu\nabla^2\mathbf{u}\,, \tag{1}$$

$$\nabla\cdot\mathbf{u} = 0\,, \tag{2}$$

where $\mathbf{u} = (u, v, w)$ is the velocity in the (x, y, z) directions, ρ is the constant density, p is the dynamic pressure, ν is the (constant eddy) kinematic viscosity, and $\nabla = (\frac{\partial}{\partial x}, \frac{\partial}{\partial y}, \frac{\partial}{\partial z})$. In addition, Nek5000 solves the advection-diffusion equation:

$$\frac{\partial C}{\partial t} + (\mathbf{u}\cdot\nabla)C = \kappa\nabla^2 C\,, \tag{3}$$

where C represents the passive scalar and κ is the scalar's diffusivity. The boundary conditions are a free surface at the top, a no-slip wall at the bottom, and periodic laterals.

We apply an impulsive surface pressure, described in Appendix A, to generate surface waves, as shown in Figure 1b. The pressure impulse exists only for a very short duration (less than 0.2 wave periods) and generates monochromatic, freely propagating surface waves that satisfy the dispersion relation of deepwater surface gravity waves.

Table 1 displays the amplitude, intrinsic frequency, and wave number of generated waves, which are deepwater ($kL_z \gg 1$) waves with small wave slope ($ka_0 = 0.112$). Variables in simulations are dimensionless (cf. Table 1): The scaling bases are 125 times wave amplitude for length, 2.5 times wave period for time, and constant water density. These waves yield a Stokes drift of $U_s = \omega k a_0^2 \sim 0.1$ m/s at the surface, observed in the sea under a wind speed around 12 m/s (e.g., Curcic et al., 2016; Van Roekel et al., 2012).

Once waves are generated, a jet-like wind stress defined by equation (4) is imposed to drive a current that has both lateral and vertical shears.

$$\tau = \tau_0\left[0.5 + 0.5\sin\left(\frac{\pi}{L_y}y\right)\right], \tag{4}$$

where τ is the wind stress in the x direction, L_y is the domain length in the y direction, and τ_0 is the maximum wind stress. With the wind stress and waves in Table 1, we have a turbulent Langmuir number $La = \sqrt{U_*/U_s} \approx 0.4$ with friction velocity of $U_* = \sqrt{\tau_0/\rho}$, which falls into the parameter regime for Langmuir circulation (e.g., M. Li et al., 2005; McWilliams et al., 1997). Besides, the downwind direction and wave propagating direction are aligned in the $+x$ direction; accordingly, the velocity components of currents in the x and y directions are called downwind velocity and crosswind velocity.

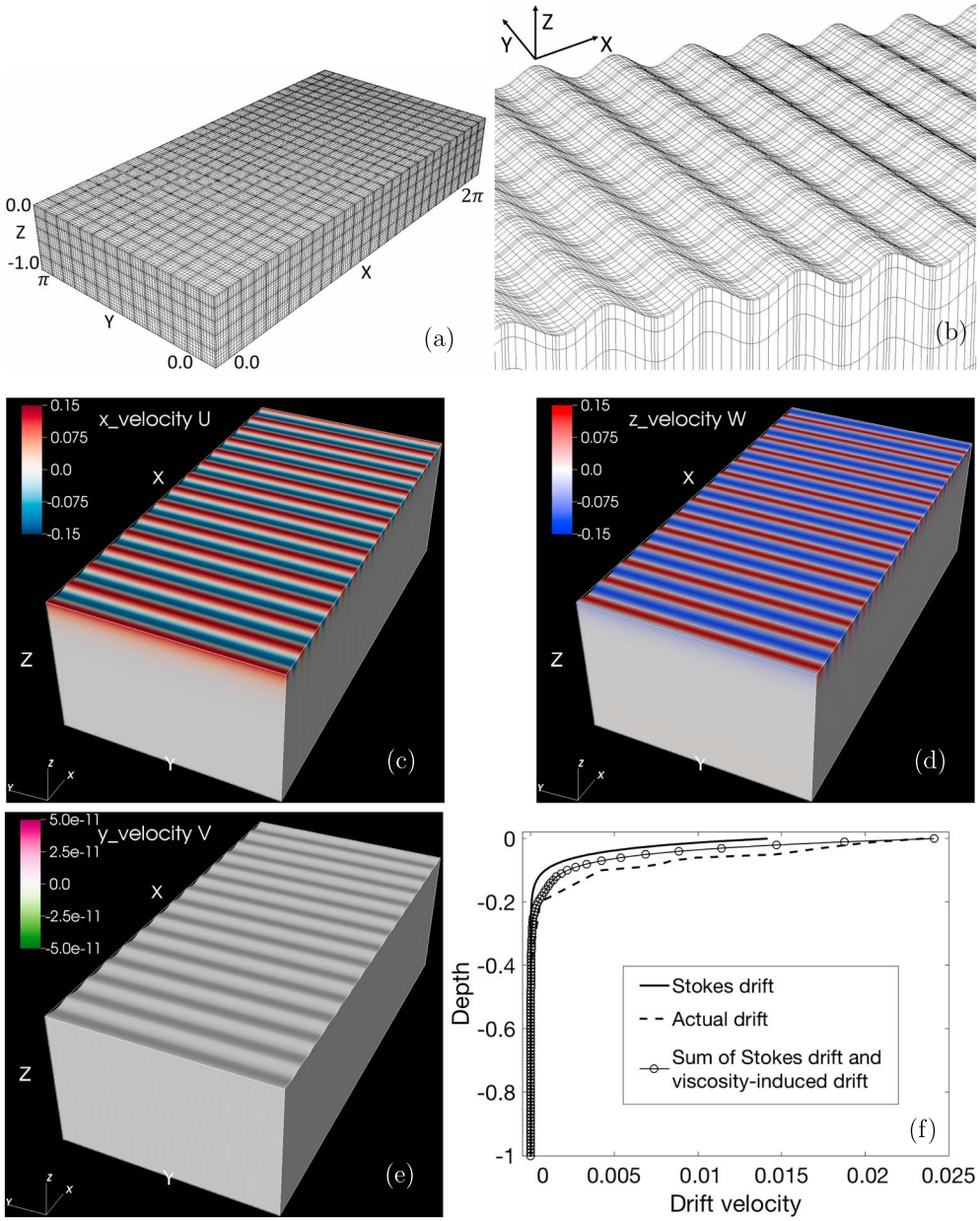

Figure 1. (a) The cuboid numerical domain consists of moving meshes. (b) Explicit surface waves modeled by moving meshes. Snapshots of the velocity fields (c) *u*, (d) *w*, and (e) *v* of the monochromatic surface waves. (f) Profiles of the drift velocities (computed after 10 wave periods).

2.2. C-L Static-Mesh Simulation

We configure Nek5000 to solve C-L equations:

$$\frac{\partial \mathbf{u}}{\partial t} + (\mathbf{u}\cdot\nabla)\mathbf{u} = -\nabla P + \mathbf{u}_s \times (\nabla \times \mathbf{u}) + \nu\nabla^2\mathbf{u}\,, \tag{5}$$

$$\nabla\cdot\mathbf{u} = 0\,, \tag{6}$$

where $\mathbf{u}$ is the Eulerian velocity averaged over surface waves, $\mathbf{u}_s$ is the Stokes drift, $\mathbf{u}_s \times (\nabla \times \mathbf{u})$ is the vortex force, and $P = p/\rho + \frac{1}{2}(|\mathbf{u}+\mathbf{u}_s|^2 - |\mathbf{u}|^2)$ is the generalized pressure (e.g., McWilliams et al., 1997). We also modify the advection-diffusion equation to include the Stokes drift; that is,

$$\frac{\partial C}{\partial t} + [(\mathbf{u}+\mathbf{u}_s)\cdot\nabla]C = \kappa\nabla^2 C\,. \tag{7}$$

Table 1
Parameters Used in Numerical Simulations: L_x, L_y, L_z Are Domain Length in the x, y, z Direction

Parameters	L_x, L_y, L_z	$\Delta x, \Delta y$	Δz	Δt
Dimensionless	$2\pi, \pi, 1$	[0.014, 0.047]	[0.01, 0.015]	0.004
Dimensional	628 m, 314 m, 100 m	[1.4 m, 4.7 m]	[1 m, 1.5 m]	0.054 s
Parameters	a_0	ω	k	τ_0
Dimensionless	0.008	15.81	14	6×10^{-6}
Dimensional	0.8 m	1.17 rad/s	0.14 m^{-1}	0.33 N/m^2

Note. Δx, Δy, and Δz are the horizontal and vertical resolution; a_0, ω, and k are the wave amplitude, intrinsic frequency, and wave number; τ_0 is the magnitude of wind stress.

Except the surface boundary which now becomes a rigid lid, other boundary conditions and initial conditions are identical to those used in the N-S moving-mesh simulation.

The Stokes drift, which only has the x component here, is calculated according to equation (8) that is derived for inviscid, irrotational, deepwater surface gravity waves:

$$u_s(x, y, z, t) = a(x, y, t)^2 \omega k e^{2kz} . \tag{8}$$

Wave number k and intrinsic frequency ω take the values in Table 1. Because the wave amplitudes $a(x, y, t)$ change constantly during the wave-current interaction, they must be calculated at every time step. We estimate the wave amplitudes in terms of

$$a(x, y, t) = \sqrt{\eta^2 + (W/\omega)^2} , \tag{9}$$

which is derived using relations of $\eta = a \sin(kx - \omega t)$ and $W = -a\,\omega \cos(kx - \omega t)$ for linear deepwater waves, with the surface elevation η and the vertical component of wave's orbital velocity W at the surface. In this study, η and W are output from the N-S moving-mesh simulation. η, W, and a vary in time and space, so does Stokes drift $u_s(x, y, z, t)$; thus, Stokes drift must be updated at every time step and every grid point.

3. Results

3.1. Profiles of Stokes Drift

First, we check the behavior of explicit surface waves simulated by the moving-mesh model (Figures 1c–1e); no wind stress is imposed at this point. Our tests show that the wave amplitude, wave number, and frequency listed in Table 1 are well maintained for about 1,600 wave periods, long enough to generate Langmuir circulation in our simulation which runs about 1,300 wave periods.

The profile of drift velocity is computed based on particle trajectories at multiple depths; this computation yields an "actual drift" that particles actually experience. In fact, the actual drift contains not only a Stokes drift but also a Eulerian mean drift, which is induced by fluid viscosity in the presence of explicit surface waves (Longuet-Higgins, 1960; Phillips, 1966). This viscosity-induced Eulerian mean drift can be obtained by phase average of waves. As shown in Figure 1f, at the surface the actual drift is about 66% larger than the Stokes drift calculated using equation (8); the profile of actual drift is very close to that of total drift, which sums the Stokes drift and viscosity-induced drift.

3.2. Formation of Langmuir Circulation

As shown in Figures 2a and 2b, waves are changed when interacting with currents, such as their amplitude, orbital velocity, and phase speed; particularly, in the surface central region where the current is stronger, the phase speed of waves is larger due to the Doppler shift, causing wave bending. In addition, the crosswind velocity is no longer nil (Figure 2c), which is crucial to form the surface convergence zone and Langmuir circulation. Large crosswind velocities appear in the surface flanks where the current is weaker and are organized into two arrays (Figure 2c).

After about 650 wave periods, the arrays of crosswind velocity move toward the surface center (Figure 2f); each array is accompanied by a downwelling, which moves with the array (Figures 2d and 2e). When the

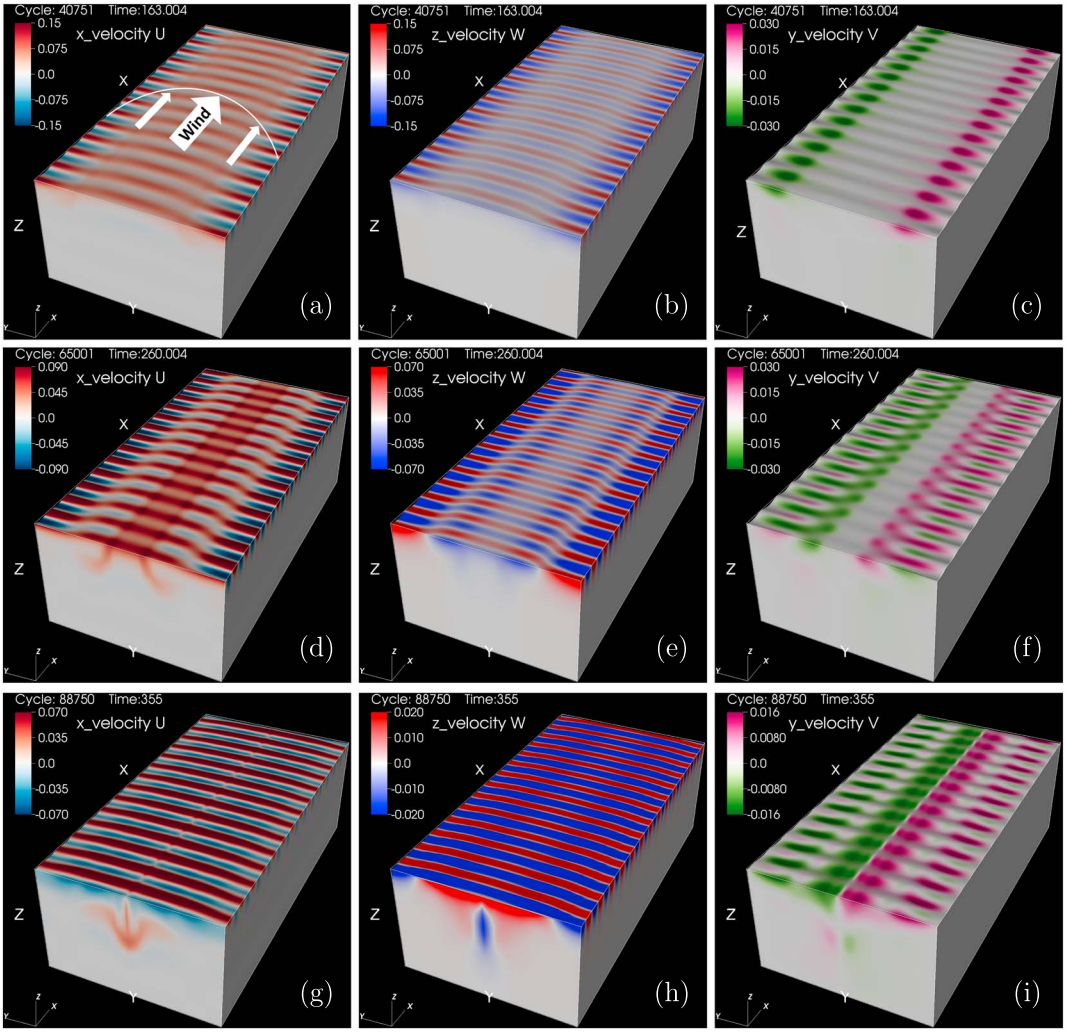

Figure 2. Formation of Langmuir circulation in the N-S moving-mesh simulation, visualized using velocity fields (a, d, and g) *u*, (b, e, and h) *w*, and (e, f, and i) *v* at time stamps equal to 408 (Figures 2a–2c), 650 (Figures 2d–2f), and 888 (Figures 2g–2i) wave periods. The white arrows shown in Figure 2a denote the jet-like wind stress. For the animation please visit https://youtu.be/F2DzWKgywdA.

two arrays meet, the two downwellings coalesce (Figures 2g and 2h), and a line of convergence forms at the surface center (Figure 2i). Outside the narrow and strong downwelling are the broad and weak upwellings, which carry up deep water to surface layers.

3.3. Comparison of Langmuir Circulations

For comparison, we also simulate the Langmuir circulation with C-L equations. Stokes drifts are calculated using equations (8) and (9) with the waves information from N-S simulation and are updated into C-L equations at every time step and grid point. Langmuir circulations between N-S and C-L simulations are compared from three aspects: (i) velocity fields associated with Langmuir circulation, (ii) transport of passive tracer by Langmuir circulation, and (iii) vortex force and radiation stress.

As shown in Figure 3, the patterns and magnitudes of velocity fields are very similar between the N-S and C-L simulations, except in the surface layers where waves dominate in the N-S simulation. According to Figures 4a and 4b, velocity magnitudes of Langmuir circulation in the C-L simulation are overall smaller (~20%). In addition, around time = 350 (875 wave periods), the downwind velocity and downwelling at the middepth suddenly jumps due to the arrival of downwelling; the jump predicted by C-L equations is delayed about 43 wave periods.

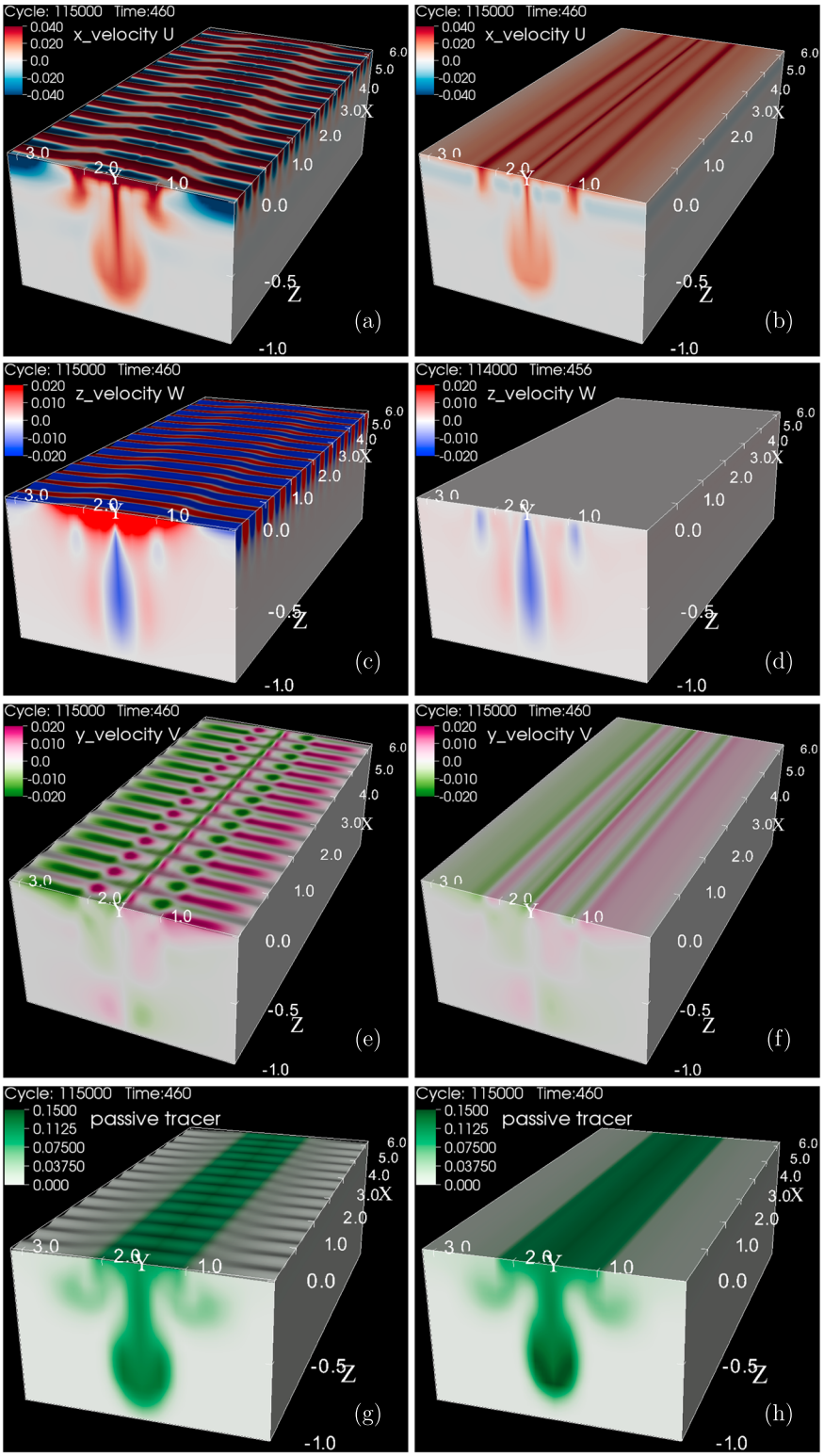

Figure 3. Comparison of the Langmuir circulation predicted by N-S equations (Figures 3a, 3c, 3e, and 3g) and C-L equations (Figures 3b, 3d, 3f, and 3h), in terms of the velocity components (a, b) *u*, (c, d) *w*, (e, f) *v*, and (g, h) passive tracer at time stamp around 1,150 wave periods.

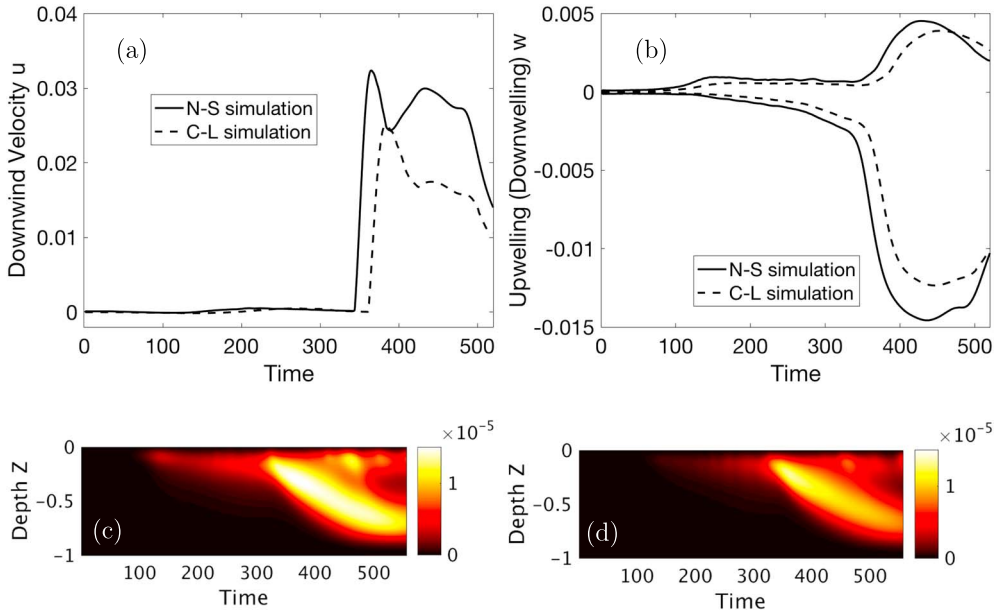

Figure 4. Evolutions of (a) the maximum downwind velocity *u* and (b) the maximum downwelling and upwelling *w* at the middepth. Hovmöller diagram of vertical TKE in the (c) N-S simulation and (d) C-L simulation.

The profile of vertical TKE of Langmuir circulation is calculated by horizontally averaging w^2 at each depth; as shown in Figures 4c and 4d, evolutions of vertical TKE show the penetration of Langmuir circulation into deep layers. The TKE profiles in both simulations are similar, including the depth and rate of TKE penetration; yet the TKE in the C-L simulation is smaller (~30%), consistent with the weaker Langmuir circulation in the C-L simulation (cf. Figures 4a and 4b).

The transport of passive tracer by Langmuir circulation is examined. At the beginning a thin layer of tracer is injected at the surface, with identical tracer concentration and diffusivity in both simulations. During the development of Langmuir circulation, the tracer is accumulated toward the surface center by the crosswind velocity, and mean time is transported down by the downwelling. According to Figures 3g and 3h, tracers in both simulations are transported in almost the same way, except that the tracer reaches deeper and mixes better in the N-S simulation.

There are two representations of wave effects on currents, that is, radiation stress (e.g., Longuet-Higgins & Stewart, 1962; Mellor, 2015; Phillips, 1966) and vortex force (e.g., Craik & Leibovich, 1976; McWilliams et al., 2004). We visualize radiation stress and vortex force to reveal their characteristics during the formation of Langmuir circulation. The vertically dependent radiation stress ($S_{\alpha\beta}$) is calculated using the equation derived by Mellor (2015) (his equation (29)), with phase averages taken along the wave propagating (x) direction. The gradient of radiation stress represents force, and its y component ($-\frac{\partial S_{yy}}{\partial y}$) is shown in Figures 5a–5c; as well, the y component of vortex force is displayed (Figures 5d–5f). Since the vortex force representation is accompanied by a Bernoulli head, which is a pressure adjustment owing to the wave setup effect (e.g., Lane et al., 2007; McWilliams et al., 2004), the associated pressure gradient forces are also added (Figures 5g–5l).

According to Figures 5d–5f, vortex force is limited near the surface; larger vortex force appears around surface convergence zones and follows the movement of arrays of crosswind velocity shown in Figure 2. Vortex force pushes surface water toward the center, forming surface convergence zones which are critical to generate Langmuir circulation. In contrast, radiation stress gradient force penetrates deeper (Figures 5a–5c) but does not follow the movement of arrays of crosswind velocity as vortex force does. After the pressure gradient force, that includes the Bernoulli head, is added into vortex force, the resultant force differs remarkably from vortex force and outlines the downwelling approximately (Figures 5j–5l); this implies that the Bernoulli head is requisite for representing wave effects (e.g., Lane et al., 2007). By contrast, the resultant force in the case of radiation stress does not change much, especially in the upper layers (Figures 5g–5i).

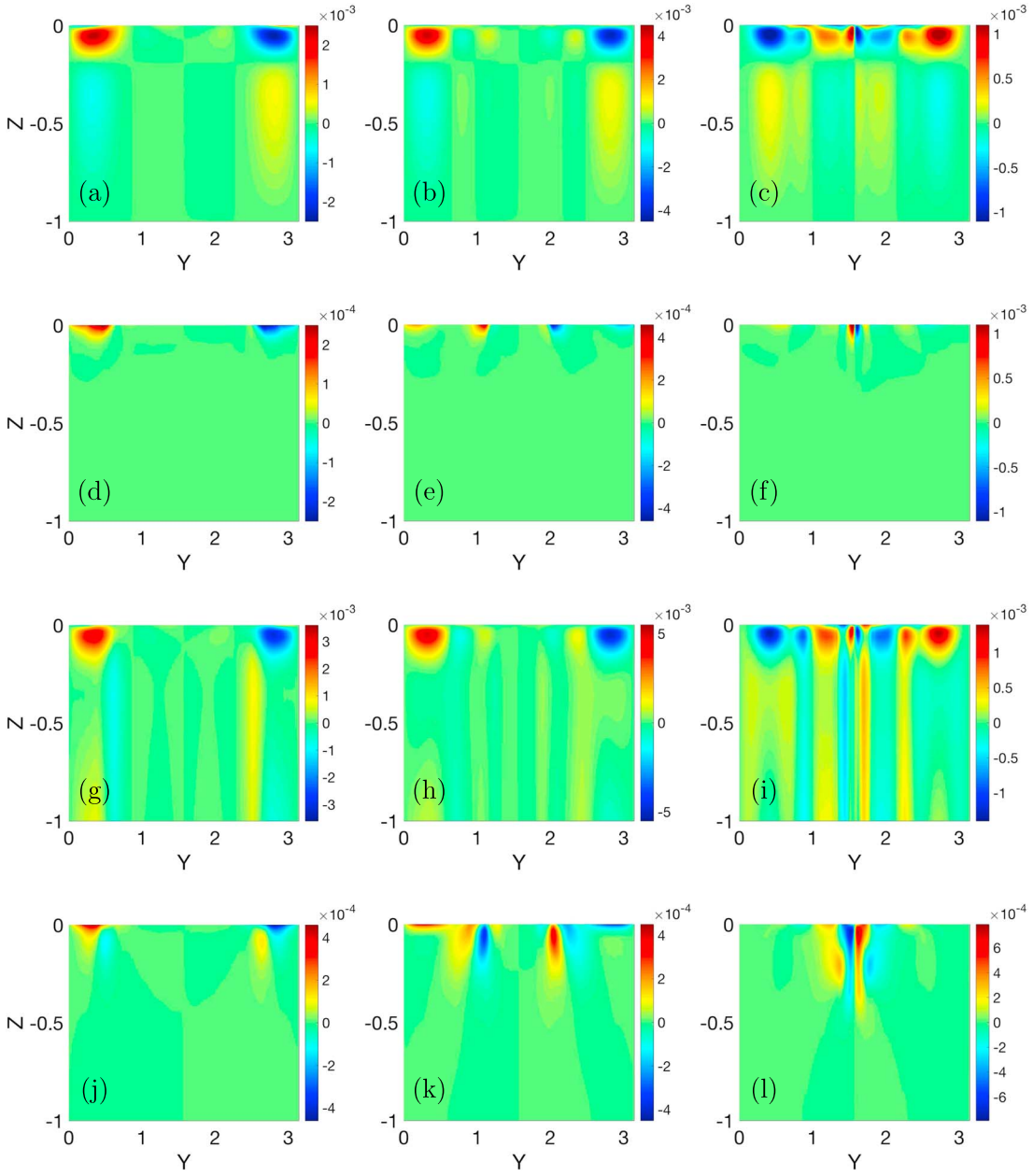

Figure 5. The (a–c) radiation stress gradient force ($-\frac{\partial S_{yy}}{\partial y}$) and (d–f) vortex force are shown; associated pressure gradient forces ($-\frac{\partial P}{\partial y}$) are added into (g–i) radiation stress gradient force and (j–l) vortex force. In particular, the pressure gradient force associated with vortex force includes a Bernoulli head. The time stamps increase from the left to the right and correspond to the time stamps of Figure 2.

4. Discussion

According to Figure 4, the strength of Langmuir circulation simulated with C-L equations is weaker, which we suggest is due to the missing of Eulerian mean drift induced by viscosity in the C-L simulation. Indeed, Zhou (2000) also found weaker Langmuir circulation in their 2-D C-L simulation without considering the viscosity-induced drift. When Zhou (2000) represented this drift by adding a surface stress (Zhou, 2000), an excellent agreement is achieved in Langmuir circulations between their 2-D C-L and 3-D N-S simulations, in both of which a constant eddy viscosity was used.

Nevertheless, using LES with a dynamic subgrid turbulence model, rather than a constant eddy viscosity, Zhou (2000) reported that C-L equations produce stronger Langmuir circulation but weaker turbulence than N-S equations do. A possible reason is that the wave averaging in C-L equations eliminates turbulences with time

scales close to the waves; in turn, stronger turbulences as in the N-S simulation weaken the coherence and strength of Langmuir circulation (Ferziger et al., 2002; Zhou, 2000).

Sullivan and McWilliams (2010) pointed out that effects of currents on waves should be addressed in using C-L equations. Our simulations confirm that in order to accurately predict Langmuir circulation with C-L equations, Stokes drift must be updated constantly based on the waves that contains effects of currents, for example, the waves directly from the N-S moving-mesh simulation. Otherwise, if Stokes drifts are assumed to be constant or are calculated using waves that has no currents effects, our tests show that the Langmuir circulation simulated with C-L equations will differ greatly from that simulated with N-S equations. In realistic ocean environments, Stokes drifts can be computed using wave spectra obtained from wave models that contain currents effects on waves.

Breaking waves are not considered in this study. Currently, wave breaking cannot be directly modeled by Nek5000, but it can be avoided by properly selecting the pressure impulse, wind stress and viscosity. In addition, Coriolis-Stokes vortex force needs to be considered for larger-scale Langmuir circulation, as this force can change the profile of wind-driven currents (e.g., Polton et al., 2005) and can provide a new way of energy transfer between waves and turbulence (e.g., Suzuki & Fox-Kemper, 2016).

Belcher et al. (2012) compared mixed layer depths from a state-of-the-art climate model with those from Argo floats and found that the climate model predicts overall shallower mixed layer depths, particularly in the Southern Ocean. One reason, Belcher et al. (2012) argue, is that parameterizations of unresolved processes in the climate model are missing Langmuir circulation which deepens mixed layer depths more rapidly than steady wind forcing. Systematic biased predictions of mixed layer depths imply incorrect predictions of momentum, heat, and trace gases exchanged between atmosphere and ocean by climate models; this will impact the long-term climate prediction. Hence, a parameterization of Langmuir circulation needs to be included into climate models, and LES based on C-L equations can guide this parameterization by comparison with field observations.

5. Conclusions

Our study provides an evidence that the Langmuir circulation simulated with C-L equations is correct compared to that simulated with N-S equations, in the context of explicit, freely propagating surface waves of small wave slopes. To ensure the accuracy of simulation with C-L equations, Stokes drifts must be calculated based on the waves that contain effects of currents; also, a Eulerian mean drift induced by fluid viscosity needs to be considered when C-L equations are used.

Appendix A: Impulsive Pressure Applied at the Free Surface

A relation between surface pressure and surface elevation can be obtained by solving the linearized Cauchy-Poisson problem of waves generated by an impulsive source (e.g., Guo & Shen, 2009; Mei et al., 2005). According to this relation, an impulsive pressure given by equation (A1) will generate freely propagating, deepwater surface gravity waves in initially calm water, in the waveform of $\eta = -a\sin(kx - \omega t)$ with the surface elevation η, amplitude a, frequency ω, and wave number k.

$$P_a = -\frac{a}{Fr^2\omega}\delta(t)\cos(kx) - \frac{a}{Fr^2\omega}\delta(t - \frac{\pi}{2\omega})\sin(kx)\,, \tag{A1}$$

where P_a is the impulsive pressure at the surface and $Fr = U/\sqrt{gL}$ is the Froude number with characteristic scales of wave velocity U and length L, and gravitational acceleration g. The Dirac $\delta(t)$ function is defined as $\delta(t) = 1$ at $t = 0$, and $\delta(t) = 0$ otherwise. To be implemented numerically, $\delta(t)$ function is modified as

$$\delta(x) = \begin{cases} \frac{1}{2\Delta}\left(1 + \cos\left[\frac{\pi}{\Delta}t\right]\right), & -\Delta < t < \Delta\,, \\ 0\,, & \text{otherwise}\,, \end{cases}$$

where Δ is a parameter that determines the width of numerical smoothing in time (Guo & Shen, 2009).

Acknowledgments
We thank the three anonymous reviewers for their constructive and helpful comments. Also, we are grateful for the financial support from the Office of Naval Research (grant N000141110087) and the Gulf of Mexico Research Initiative. Model data can be accessed from the GRIIDC repository (https://data.gulfresearchinitiative.org/dataset-monitoring).

References

Andrews, D. G., & McIntyre, M. E. (1978). An exact theory of nonlinear waves on a Lagrangian-mean flow. *Journal of Fluid Mechanics*, *89*(4), 609–646.

Ardhuin, F., Rascle, N., & Belibassakis, K. A. (2008). Explicit wave-averaged primitive equations using a generalized Lagrangian mean. *Ocean Modelling*, *20*(1), 35–60.

Belcher, S. E., Grant, A. L. M., Hanley, K. E., Fox-Kemper, B., Van Roekel, L., Sullivan, P. P., … Polton, J. A. (2012). A global perspective on Langmuir turbulence in the ocean surface boundary layer. *Geophysical Research Letters*, *39*, L18605. https://doi.org/10.1029/2012GL052932

Craik, A. D., & Leibovich, S. (1976). A rational model for Langmuir circulations. *Journal of Fluid Mechanics*, *73*(3), 401–426.

Curcic, M., Chen, S. S., & Özgökmen, T. M. (2016). Hurricane-induced ocean waves and Stokes drift and their impacts on surface transport and dispersion in the Gulf of Mexico. *Geophysical Research Letters*, *43*, 1–9. https://doi.org/10.1002/2015GL067619

D'Asaro, E. A., Thomson, J., Shcherbina, A. Y., Harcourt, R. R., Cronin, M. F., Hemer, M. A., & Fox-Kemper, B. (2014). Quantifying upper ocean turbulence driven by surface waves. *Geophysical Research Letters*, *41*, 102–107. https://doi.org/10.1002/2013GL058193

Ferziger, J. H., Koseff, J. R., & Monismith, S. G. (2002). Numerical simulation of geophysical turbulence. *Computers and Fluids*, *31*(4), 557–568.

Fischer, P. F. (1997). An overlapping Schwarz method for spectral element solution of the incompressible Navier-Stokes equations. *Journal of Computational Physics*, *133*(1), 84–101.

Gargett, A., Wells, J., Tejada-Martínez, A. E., & Grosch, C. E. (2004). Langmuir supercells: A mechanism for sediment resuspension and transport in shallow seas. *Science*, *306*(5703), 1925–1928.

Gargett, A. E., & Wells, J. R. (2007). Langmuir turbulence in shallow water: Part 1. Observations. *Journal of Fluid Mechanics*, *576*, 27–61.

Gargett, A. E., Savidge, D. K., & Wells, J. R. (2014). Anatomy of a Langmuir supercell event. *Journal of Marine Research*, *72*(3), 127–163.

Gjaja, I., & Holm, D. D. (1996). Self-consistent Hamiltonian dynamics of wave mean-flow interaction for a rotating stratified incompressible fluid. *Physica D: Nonlinear Phenomena*, *98*, 343–378.

Guo, X., & Shen, L. (2009). On the generation and maintenance of waves and turbulence in simulations of free-surface turbulence. *Journal of Computational Physics*, *228*(19), 7313–7332.

Harcourt, R. R., & D'Asaro, E. A. (2008). Large-eddy simulation of Langmuir turbulence in pure wind seas. *Journal of Physical Oceanography*, *38*(7), 1542–1562.

Holm, D. D. (1996). The ideal craik-leibovich equations. *Physica D: Nonlinear Phenomena*, *98*, 415–441.

Kawamura, T. (2000). Numerical investigation of turbulence near a sheared air–water interface. Part 2: Interaction of turbulent shear flow with surface waves. *Journal of Marine Science and Technology*, *5*(4), 161–175.

Kukulka, T., Plueddemann, A. J., Trowbridge, J. H., & Sullivan, P. P. (2009). Significance of Langmuir circulation in upper ocean mixing: Comparison of observations and simulations. *Geophysical Research Letters*, *36*, L10603. https://doi.org/10.1029/2009GL037620

Lane, E. M., Restrepo, J. M., & McWilliams, J. C. (2007). Wave–current interaction: A comparison of radiation-stress and vortex-force representations. *Journal of Physical Oceanography*, *37*(5), 1122–1141.

Langmuir, I. (1938). Surface motion of water induced by wind. *Science*, *87*(2250), 119–123.

Leibovich, S. (1983). The form and dynamics of Langmuir circulations. *Annual Review of Fluid Mechanics*, *15*(1), 391–427.

Li, M., Garrett, C., & Skyllingstad, E. (2005). A regime diagram for classifying turbulent large eddies in the upper ocean. *Deep Sea Research Part I: Oceanographic Research Papers*, *52*(2), 259–278.

Li, S., Li, M., Gerbi, G. P., & Song, J. B. (2013). Roles of breaking waves and Langmuir circulation in the surface boundary layer of a coastal ocean. *Journal of Geophysical Research: Oceans*, *118*, 5173–5187. https://doi.org/10.1002/jgrc.20387

Longuet-Higgins, M. S. (1960). Mass transport in the boundary layer at a free oscillating surface. *Journal of Fluid Mechanics*, *8*(2), 293–306.

Longuet-Higgins, M. S., & Stewart, R. W. (1962). Radiation stress and mass transport in gravity waves, with application to 'surf beats'. *Journal of Fluid Mechanics*, *13*(4), 481–504.

McWilliams, J. C., & Restrepo, J. M. (1999). The wave-driven ocean circulation. *Journal of Physical Oceanography*, *29*(10), 2523–2540.

McWilliams, J. C., Restrepo, J. M., & Lane, E. M. (2004). An asymptotic theory for the interaction of waves and currents in coastal waters. *Journal of Fluid Mechanics*, *511*, 135–178.

McWilliams, J. C., & Sullivan, P. P. (2000). Vertical mixing by Langmuir circulations. *Spill Science and Technology Bulletin*, *6*(3), 225–237.

McWilliams, J. C., Sullivan, P. P., & Moeng, C. H. (1997). Langmuir turbulence in the ocean. *Journal of Fluid Mechanics*, *334*(1), 1–30.

Mei, C. C., Stiassnie, M., & Yue, D. K. P. (2005). *Theory and Applications of Ocean Surface Waves: Part 1: Linear Aspects*. Singapore: World Scientific.

Mellor, G. (2015). A combined derivation of the integrated and vertically resolved, coupled wave-current equations. *Journal of Physical Oceanography*, *45*(6), 1453–1463.

Mellor, G. (2016). On theories dealing with the interaction of surface waves and ocean circulation. *Journal of Geophysical Research: Oceans*, *121*, 4474–4486. https://doi.org/10.1002/2016JC011768

Melville, W. K. (1996). The role of surface-wave breaking in air-sea interaction. *Annual Review of Fluid Mechanics*, *28*(1), 279–321.

Noh, Y., Min, H. S., & Raasch, S. (2004). Large eddy simulation of the ocean mixed layer: The effects of wave breaking and Langmuir circulation. *Journal of Physical Oceanography*, *34*(4), 720–735.

Patera, A. T. (1984). A spectral element method for fluid dynamics: Laminar flow in a channel expansion. *Journal of Computational Physics*, *54*(3), 468–488.

Phillips, O. M. (1966). *The Dynamics of The Upper Ocean*. Cambridge, UK: Cambridge Press.

Polton, J. A., Lewis, D. M., & Belcher, S. E. (2005). The role of wave-induced Coriolis-Stokes forcing on the wind-driven mixed layer. *Journal of Physical Oceanography*, *35*(4), 444–457.

Pratt, L. J., Rypina, I. I., Özgökmen, T. M., Wang, P., Childs, H., & Bebieva, Y. (2014). Chaotic advection in a steady, three-dimensional, Ekman-driven eddy. *Journal of Fluid Mechanics*, *738*, 143–183.

Rypina, I. I., Pratt, L. J., Wang, P., Özgökmen, T. M., & Mezic, I. (2015). Resonance phenomena in a time-dependent, three-dimensional model of an idealized eddy. *Chaos: An Interdisciplinary Journal of Nonlinear Science*, *25*(8), 087401.

Skyllingstad, E. D., & Denbo, D. W. (1995). An ocean large-eddy simulation of Langmuir circulations and convection in the surface mixed layer. *Journal of Geophysical Research: Oceans*, *100*(C5), 8501–8522.

Smith, J. A. (2001). Observations and theories of Langmuir circulation: A story of mixing, *Fluid mechanics and the environment: Dynamical approaches, Lecture Notes in Physics* (Vol. 566). Berlin: Springer.

Sullivan, P. P., & McWilliams, J. C. (2010). Dynamics of winds and currents coupled to surface waves. *Annual Review of Fluid Mechanics*, *42*, 19–42.

Sullivan, P. P., McWilliams, J. C., & Melville, W. K. (2004). The oceanic boundary layer driven by wave breaking with stochastic variability: Part 1. Direct numerical simulations. *Journal of Fluid Mechanics*, *507*, 143–174.

Sullivan, P. P., McWilliams, J. C., & Melville, W. K. (2007). Surface gravity wave effects in the oceanic boundary layer: Large-eddy simulation with vortex force and stochastic breakers. *Journal of Fluid Mechanics*, *593*, 405–452.

Suzuki, N., & Fox-Kemper, B. (2016). Understanding Stokes forces in the wave-averaged equations. *Journal of Geophysical Research: Oceans*, *121*, 3579–3596. https://doi.org/10.1002/2015JC011566

Thorpe, S. A. (2004). Langmuir circulation. *Annual Review of Fluid Mechanics*, *36*, 55–79.

Uchiyama, Y., McWilliams, J. C., & Shchepetkin, A. F. (2010). Wave-current interaction in an oceanic circulation model with a vortex-force formalism: Application to the surf zone. *Ocean Modelling*, *34*, 16–35.

Van Roekel, L. P., Fox-Kemper, B., Sullivan, P. P., Hamlington, P. E., & Haney, S. R. (2012). The form and orientation of Langmuir cells for misaligned winds and waves. *Journal of Geophysical Research*, *117*, C05001. https://doi.org/10.1029/2011JC007516

Wang, P., & Özgökmen, T. M. (2015). How do hydrodynamic instabilities affect 3D transport in geophysical vortices?*Ocean Modelling*, *87*, 48–66.

Wang, P., & Özgökmen, T. M. (2016). Spiral inertial waves emitted from geophysical vortices. *Ocean Modelling*, *99*, 22–42.

Wang, P., Özgökmen, T. M., & Haza, A. C. (2016). Material dispersion by oceanic internal waves. *Environmental Fluid Mechanics*, 1–23.

Yang, D., Chamecki, M., & Meneveau, C. (2014). Inhibition of oil plume dilution in Langmuir ocean circulation. *Geophysical Research Letters*, *41*, 1632–1638. https://doi.org/10.1002/2014GL059284

Zhou, H. (2000). Numerical simulation of Langmuir circulations in a wavy domain and its comparison with the Craik-Leibovich theory. *ProQuest Dissertations and Theses*, *61-02*, 1055.